ISSN 2072-5981
doi: 10.26907/mrsej

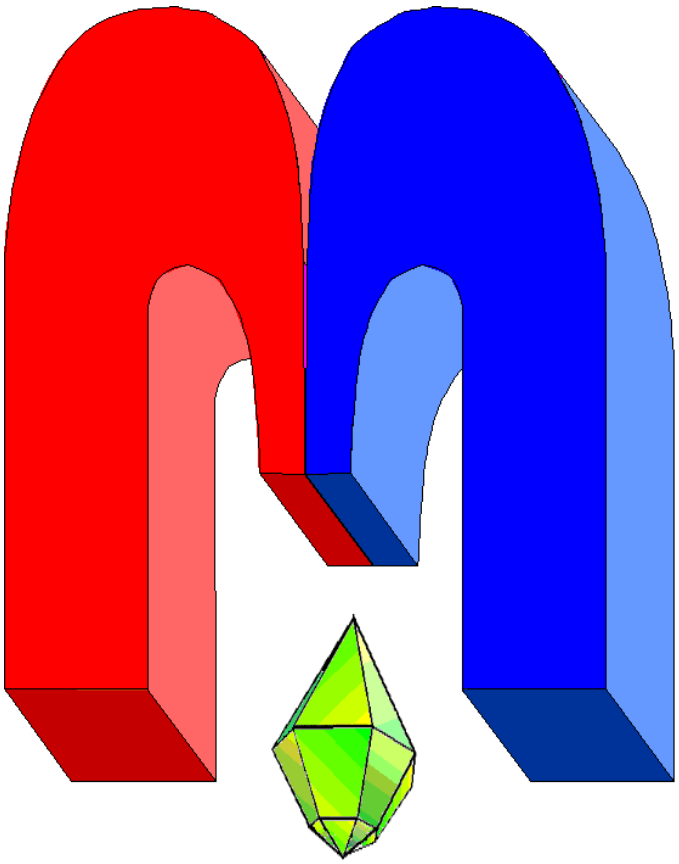

Magnetic Resonance in Solids

Electronic Journal

Volume ***26***
Issue ***1***
Article No ***24106***
1-9 pages
April, ***19***
2024
doi: **10.26907/mrsej-24106**

http://mrsej.kpfu.ru
https://mrsej.elpub.ru

Established and published by Kazan University*
Endorsed by International Society of Magnetic Resonance (ISMAR)
Registered by Russian Federation Committee on Press (#015140), August 2, 1996
First Issue appeared on July 25, 1997

© Kazan Federal University (KFU)†

"***Magnetic Resonance in Solids. Electronic Journal***" (**MRS*ej***) is a peer-reviewed, all electronic journal, publishing articles which meet the highest standards of scientific quality in the field of basic research of a magnetic resonance in solids and related phenomena.

Indexed and abstracted by
Web of Science (*ESCI*, Clarivate Analytics, from 2015), *Scopus* (Elsevier, from 2012), *RusIndexSC* (*eLibrary*, from 2006), *Google Scholar*, *DOAJ*, *ROAD*, *CyberLeninka* (from 2006), *SCImago Journal & Country Rank*, etc.

Editor-in-Chief
Boris **Kochelaev** (KFU, Kazan)

Honorary Editors
Jean **Jeener** (Universite Libre de Bruxelles, Brussels)
Raymond **Orbach** (University of California, Riverside)

Executive Editor
Yurii **Proshin** (KFU, Kazan)
mrsej@kpfu.ru

This work is licensed under a Creative Commons Attribution-ShareAlike 4.0 International License.

This is an open access journal which means that all content is freely available without charge to the user or his/her institution. This is in accordance with the BOAI definition of open access.

Technical Editor
Maxim **Avdeev** (KFU, Kazan)

Editors
Vadim **Atsarkin** (Institute of Radio Engineering and Electronics, Moscow)
Yurij **Bunkov** (CNRS, Grenoble)
Mikhail **Eremin** (KFU, Kazan)
David **Fushman** (University of Maryland, College Park)
Hugo **Keller** (University of Zürich, Zürich)
Yoshio **Kitaoka** (Osaka University, Osaka)
Boris **Malkin** (KFU, Kazan)
Alexander **Shengelaya** (Tbilisi State University, Tbilisi)
Jörg **Sichelschmidt** (Max Planck Institute for Chemical Physics of Solids, Dresden)
Haruhiko **Suzuki** (Kanazawa University, Kanazava)
Murat **Tagirov** (KFU, Kazan)
Dmitrii **Tayurskii** (KFU, Kazan)
Valentine **Zhikharev** (KNRTU, Kazan)

* Address: "Magnetic Resonance in Solids. Electronic Journal", Kazan Federal University; Kremlevskaya str., 18; Kazan 420008, Russia

† In Kazan University the Electron Paramagnetic Resonance (EPR) was discovered by Zavoisky E.K. in 1944.

Short cite this: *Magn. Reson. Solids* **26**, 24106 (2024) doi: 10.26907/mrsej-24106

DFT investigation of magneto-electric coupling at the antiferromagnetic/ferroelectric interfaces: $LaMnO_3/XTiO_3$ (X=Ba, Pb) heterostructure†

I.I. Piyanzina[1,2,*], R.F. Mamin[2], O.V. Nedopekin[1], D.A. Tayurskii[1]

[1]Kazan Federal University, Kazan 420008, Russia

[2]Zavoisky Physical-Technical Institute, FRC Kazan Scientific Center of RAS, Kazan 420029, Russia

**E-mail: i.piyanzina@gmail.com*

(Received March 15, 2024; accepted April 15, 2024; published April 19, 2024)

The primary benefit of incorporating a ferroelectric material into a complex heterostructure lies in the ability to manipulate various properties of the entire system using an external electric field. Specifically, the electric field can alter the polarization direction within the ferroelectric material, thereby influencing its structural properties. These structural changes, in turn, affect the electronic and magnetic properties of the neighboring material. The interfacial phenomena are of significant interest due to their potential to provide enhanced functionality in next-generation electronic devices. Inspired by the concept of employing ferroelectrics in heterostructure components, this study investigates the two-dimensional electron gas (2DEG) and the impact of ferroelectric polarization direction onto the electronic and magnetic properties. Lastly the presence of magnetoelectric coupling (ME) within the model systems of $LaMnO_3/BaTiO_3$ and $LaMnO_3/PbTiO_3$ heterostructures using density functional theory calculations was examined.

PACS: 73.20.-r, 73.20.At

Keywords: ferroelectric, heterostructure, density functional theory, 2DEG, ME coupling.

1. Introduction

Incorporating a ferroelectric component into a heterostructure introduces novel and remarkable functionalities that can be harnessed in advanced electronic devices. It is well-known that the emergence of a two-dimensional electron gas or liquid (2DEG or 2DEL) can be attributed to the presence of internal electrical polarization. In the case of most known heterostructure $LaAlO_3/SrTiO_3$ the internal polarization arises from the charge sequence in $LaAlO_3$ atomic layers. Notably, the presence of spontaneous polarization in ferroelectric thin films can also lead to the formation of a 2DEG, even in the absence of charged atomic layers [1–6]. This implies that the electronic and magnetic properties of the resulting state can be manipulated by applying an external field, which alters the orientation of the ferroelectric dipoles.

Another feature that holds promise for electronic applications is (ME) magnetoelectric and reverse ME coupling. This feature causes the ability to control ferromagnetic ordering at the interface through interactions between spins mediated by conduction electrons, giving rise to multiferroic properties within the heterostructure. Multiferroic materials are compounds that exhibit coexistence of multiple order parameters within the same phase. A particularly intriguing and rare group among these is ferroelectric ferromagnets, which have garnered significant research interest due to their unique physical characteristics and potential for novel multifunctional devices. The allure of magnetoelectric materials lies in the possibility of manipulating magnetic properties using an external electric field [7–11]. Given the formidable challenge of synthesizing multiferroic compounds, researchers turned to the development of superlattice multicomponent

†This paper is dedicated to Professor Boris I. Kochelaev on the occasion of his 90th birthday.

multiferroic materials. These materials comprise a magnetic insulator, which facilitates the formation of spin-polarized two-dimensional electron gases (2DEGs), and a ferroelectric component, which enables the manipulation of the magnetic state via an electric field. This approach effectively realizes the converse magnetoelectric (ME) effect.

The current research employs *ab initio* calculations based on density functional theory (DFT) to investigate heterostructures composed of ferroelectric materials ($BaTiO_3$ or $PbTiO_3$) and the antiferromagnetic compound $LaMnO_3$. Similar systems were investigated before, the examples might be found in Refs. [4, 12–14]. The common feature of these works is the use of antiferromagnet (AFM) as a source of magnetism and ferroelectric (FE) to manipulate the interfacial states. The primary objective is to elucidate the electronic and magnetic states that arise at the interfaces of these heterostructures and to explore the potential for controlling interfacial properties (such as the formation of two-dimensional electron gases and magnetoelectric coupling) by manipulating ferroelectric polarization. The paper is structured as follows: an introductory section provides background information, followed by a short presentation of data on the bulk properties of the constituent compounds. Subsequently, the results for the bare fully optimized heterostructures are presented, including spin- and atom-resolved density of states (DOS) plots. The investigation culminates with an examination of the effects of various polarization directions on the heterointerface properties.

2. Method and calculation parameters

This research employed density functional theory [15] to investigate the structural, electronic, and magnetic properties of $LaMnO_3/BaTiO_3$ and $LaMnO_3/PbTiO_3$ heterostructures. The generalized gradient approximation (GGA-PBE) [16] was used to account for exchange and correlation effects. The Kohn-Sham equations [17] were solved using projected augmented wave potentials and wave functions [18]. All calculations were performed using the VASP-5.4 (Vienna *Ab-initio* Simulation Package) program [19] integrated into the MedeA computational software [20]. The plane wave cutoff energy was set to 400 eV, and the convergence criterion for atomic relaxation was 0.02 eV/Å. Self-consistent calculations were converged to an accuracy of 10^{-5} eV. Brillouin zones were sampled using Monkhorst-Pack grids [21–23], with $7\times7\times1$ **k**-points employed for each specific heterostructure. Gaussian smearing was applied with a width of 0.05 eV. To enhance the accuracy of the calculations, a simplified $+U$ correction was implemented [24]. This correction is commonly used to improve the description of electronic properties in systems with strongly correlated electrons. In this work, additional U values were applied to electrons in d and f orbitals, as suggested in Ref. [25–27]. Specifically, $U = 4.4$ and 4 eV were applied to the $3d$ orbitals of Ti and Mn, respectively, while $U = 8$ eV was applied to the $4f$ orbitals of La. The use of this correction is crucial for accurately capturing the magnetic state and band gaps of the materials.

The heterostructure models were constructed with $BaTiO_3$ (BTO) or $PbTiO_3$ (PTO) overlayer on $LaMnO_3$ (LMO) substrate. The unit cell of the investigated structures is presented in Figure 1. No vacuum region was introduced to minimize surface effects. Prior to investigating the heterostructures, the formation energies were calculated to assess their stability among different possible surface stackings. The most stable interface configurations were selected for further analysis.

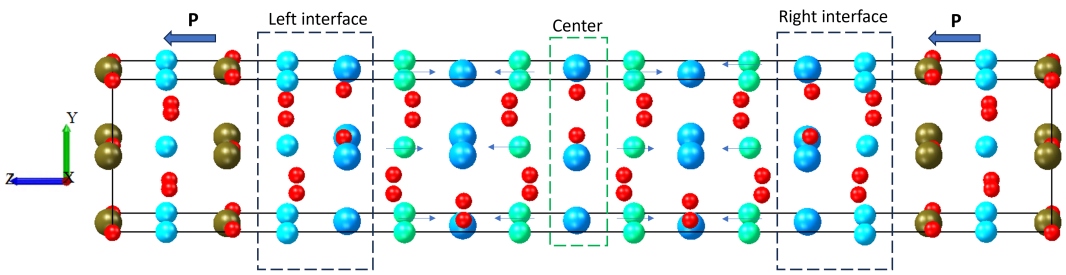

Figure 1. The unit cell of a studied optimized $(LMO)_{4.5}/(BTO)_{3.5}$ heterostructure along with denoted polarization directions arose after the optimization (big dark blue arrows) and magnetic moments (narrow light blue arrows).

3. Results

As was mentioned in the introduction a 2DEG can arise at the interface of non-polar insulative oxides, provided that one of the materials is ferroelectric [1]. This mechanism offers the potential for switchable conductivity, as the 2DEG can be controlled by an external electric field.

3.1. Structural, electronic and magnetic characteristics

Indeed, the bulk components of both studied systems are insulators: LMO is an antiferromagnet with A-type ordering, while BTO and PTO are ferroelectrics in the tetragonal phase [29, 30]. PTO exhibits stronger ferroelectric properties than BTO, as evidenced by the larger displacement of the Ti atom out of the O-plane (0.2 Å for BTO and 0.24 Å for PTO in the bulk). More precise bulk structures properties along with comparison with available experimental data for BTO and LMO can be found in Ref. [31].

In order to construct the heterostructure it is required to merge two bulk components: BTO (PTO) and LMO, which have a significant mismatch of lattice parameters in our case. That is why we followed the procedure of of rotating the BTO overlayer by 45 degrees as was explained in Refs. [31]. Indeed, the resulted heterostructure has a mismatch of components less than 1.5%.

The constructed model of the heterostructure (Figure 1) is symmetrical with respect to the center in terms of atomic layers, but not with respect to the final atomic positions, which have changed during the optimization. The structural distortions and buckling within the atomic layers are associated with out of oxygen planes displacements of Ti and Ba (Pb) being most pronounced near the interface. These out-of-plane shifts contribute to the build-up of potential along the ferroelectric overlayer, giving rise to an internal electric field. Namely, the electrostatic field is directed towards the interfaces. To be more precise, on the left interface it is directed from left to right, whereas on the right side of the heterostructure it is directed from right to left as demonstrated in Figure 1 by polarization vectors. That also coincide with Figure 2, where the average potential distribution along the heterostructure is presented. It is seen from the plot that ferroelectric slabs have higher potentials. Besides, one can notice that the potential fluctuations in BTO are smaller than in PTO due to the stronger ferroelectric nature of the last one. Lastly, such distribution of potential and electric field results in the electronic reconstruction resulting in the accumulation of electrons in the LMO slab. The latest was also confirmed by calculating the electron localization function (ELF) demonstrated in Figure 3, which denotes the probability of encountering an electron within the spatial vicinity of a designated electron positioned at a specific point and having the same spin.

As seen from the optimized structure the two interfaces are not identical in terms of po-

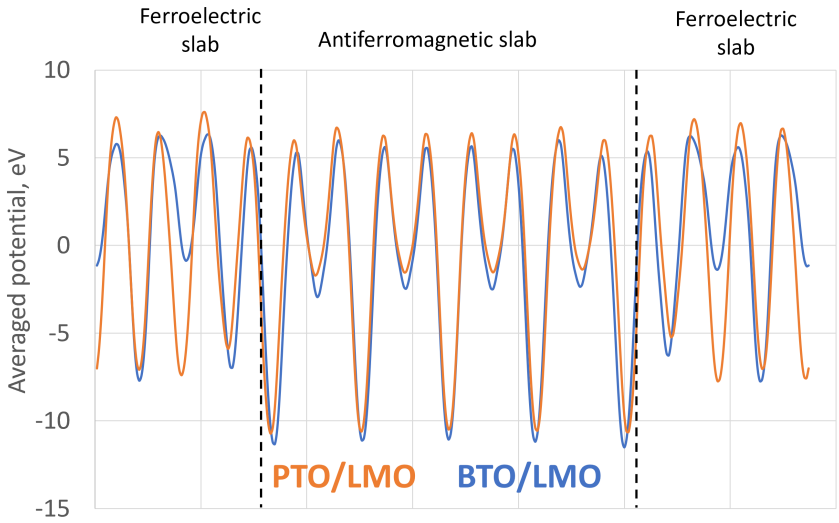

Figure 2. Average effective single-particle potential distribution along the $(LMO)_{4.5}/(BTO)_{3.5}$ and $(LMO)_{4.5}/(PTO)_{3.5}$ heterostructures as presented in Figure 1.

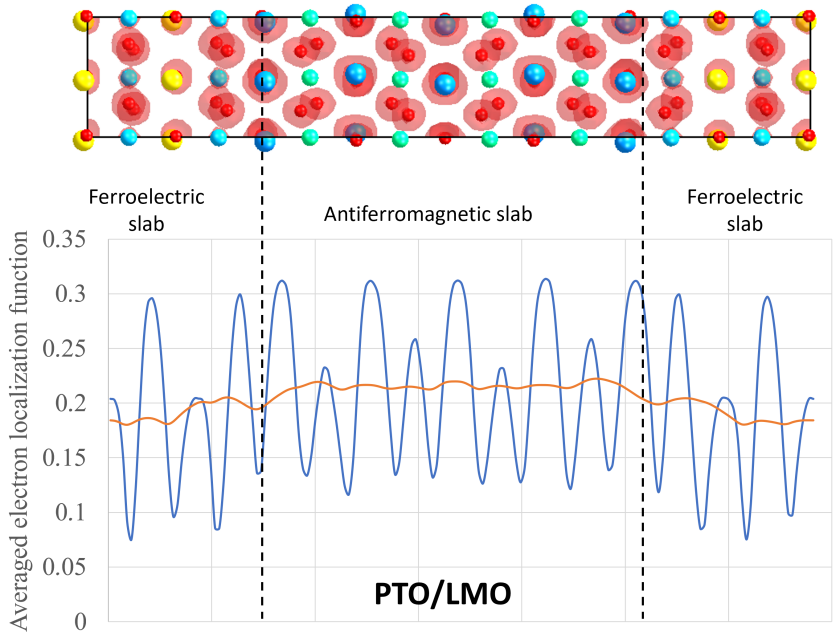

Figure 3. The electron localization functions (ELF) calculated for the $(LMO)_{4.5}/(PTO)_{3.5}$ heterostructures as presented by 3D isosurfaces (upper plot) and (bottom plot) average ELF distribution along the slab demonstrated by blue curve. The smooth orange curve was generated from the original one by proper broadening to allow for a better analysis of the overall trend.

larization and magnetic moments direction. As for the left interface the resulted polarization and initial magnetic moment have an opposite directions, whereas the right interface possesses co-directed vectors. The fact that the initially BTO (PTO) film without LMO was in the paraelectric state allows us to conclude that the spin-induced ferroelectricity takes place here. Additional reason for that conclusion is the significant ferroelectric-type displacement of Ba(Pb) and Ti out of the oxygen planes near the interfaces, which decreases while moving away from it. The presented reasoning is true for both BTO and PTO overlayered heterostructures. The difference is in the magnitude of out of plane displacements, which is higher in the PTO due to stronger ferroelectric features of that material.

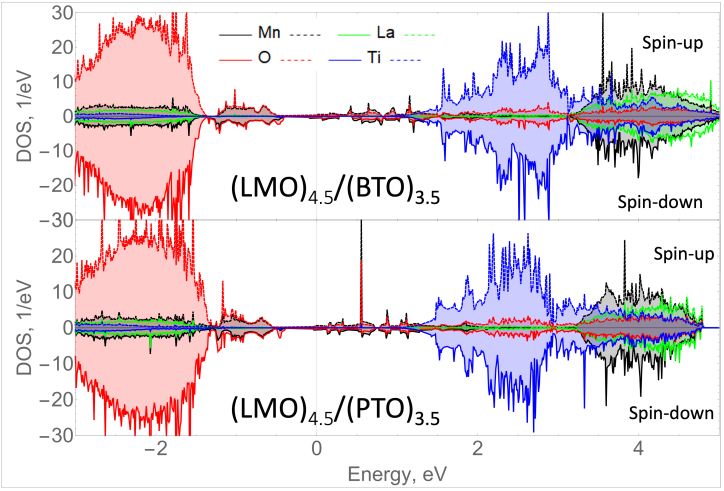

Figure 4. Atom-resolved density of states (DOS) of two interfaces of $(LMO)_{4.5}/(BTO)_{3.5}$ and $(LMO)_{4.5}/(PTO)_{3.5}$ heterostructures as presented in Figure 1.

In order to analyze the arising electronic and magnetic states the spin-polarized calculation of density of states (DOS) was performed for both studied heterostructures $(LMO)_{4.5}/(BTO)_{3.5}$ and $(LMO)_{4.5}/(PTO)_{3.5}$ after full optimization. The atom- and spin resolved DOS plots are collected in Figure 4 for both studied heterointerfaces.

The calculated density of states distribution exhibit metallic type of conductivity in contrast to the bulk properties of components. To be more precise, for LMO/BTO the DOS at the Fermi-level is slightly above zero: 0.7123 and 1.297 $[\text{eV}]^{-1}$ for spin up and down, respectively. Besides, close to the Fermi-level the main contribution is from oxygen and manganese ions located mainly within the interface atomic layer.

As for the magnetization in the optimized geometries it might be concluded the following: the initial magnetic antiferromagnetic ordering assign pre-optimization resume during it. However, the total magnetic moment of the cell in slightly above zero. Moreover, the magnetic moments of Mn ion within the LMO slab are slightly different as well as Ti ions receive magnetic moments as summarized in Table 1. We might see that the magnitudes of magnetic moments for both Mn and Ti ions are slightly higher in the LMO/PTO superlattice. Besides, the magnetic moments of interfacial Mn ions are higher that of inner ones. Moreover, within the $(TiO_2)_2$ interfacial layer the higher magnetic moment corresponds to the closest to the LMO slab Ti ion. Thus, the above confirms the presence of electromagnetic coupling.

Table 1. Distribution of magnetic moments in $(LMO)_{4.5}/(BTO)_{3.5}$ and $(LMO)_{4.5}/(PTO)_{3.5}$ heterostructures. Magnetic moments in μ_B are presented for all Mn and interfacial Ti ions, so that m1 and m4 correspond to interfacial moments, whereas m2 and m3 correspond to inner Mn ions. The signs of moments are given with respect to the z-axis as denoted in Figure 1. Two values in the cell means that the moments for two ions within the atomic layer are not identical.

supercell	ion	m1	m2	m3	m4
LMO/BTO	Mn	$-4.099/-4.065$	3.857	-3.854	4.036
	Ti	$-0.917/-0.043$	–	–	0.016
LMO/PTO	Mn	-4.070	3.875	-3.875	4.062
	Ti	$-0.052/-0.925$	–	–	0.026

3.2. Analysis of polarization impact onto the electronic and magnetic state

Starting with paraelectric state, when no optimization was performed, let's analyze each case of various possibly directed polarizations when optimization is performed keeping the ferroelectric layers frozen. In order to investigate the impact of polarization direction onto the electronic and magnetic state the DOS spectra were also plotted for two interfaces separately in Figure 5.

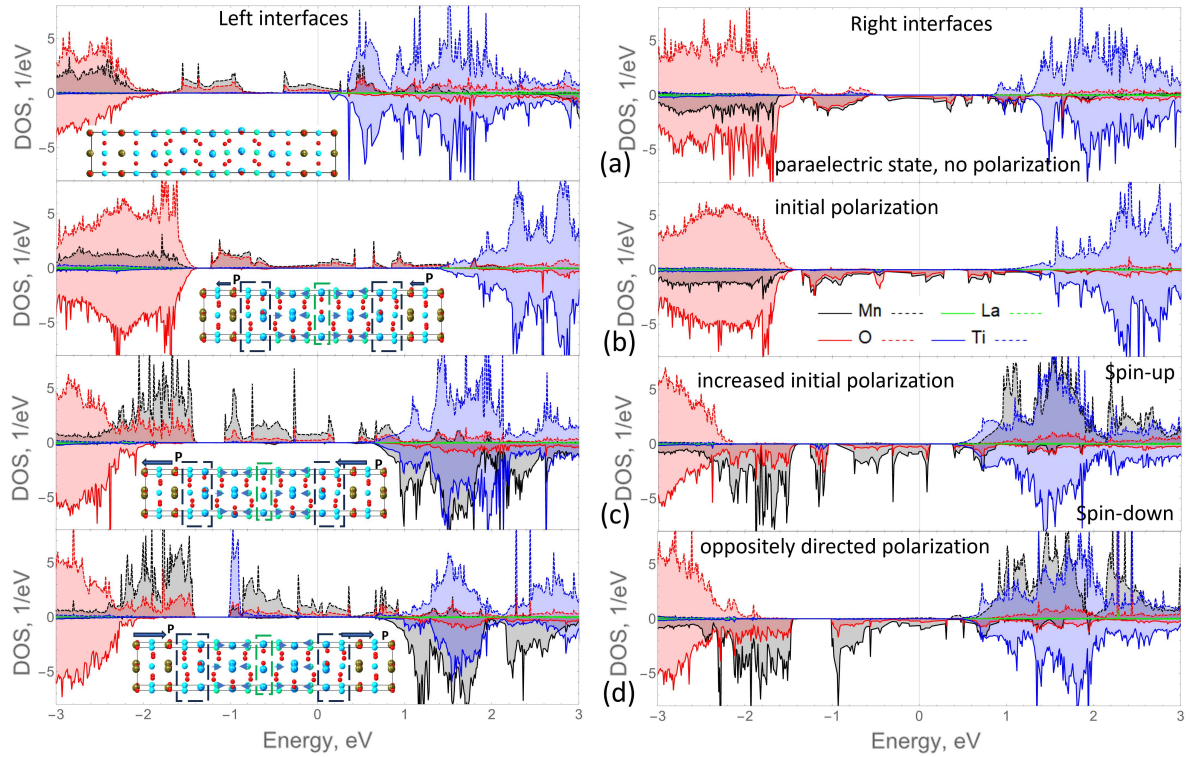

Figure 5. Atom-resolved density of states (DOS) of $(LMO)_{4.5}/(PTO)_{3.5}$ heterostructures as presented in Figure 1: (a) for a paraelectric state of PTO with no structural displacements and Pb and Ti atoms locating within one atomic layers with oxygen; (b) for a fully optimized atomic positions and corresponding polarization directed from right to left as denoted by blue arrows; (c) for an increased magnitude of polarization having direction as in the fully optimized heterostructure; (d) for an oppositely directed polarization with magnitude as in the (c) case.

Figure 5(a) shows the DOS for two interfaces separately of the ideal LMO/PTO heterostructure with no structural relaxation. That situation correspond to the metallic type of conductivity for both interfaces. Importantly, while both interfaces are identical in terms of composition, the electronic states are different. The following features are present: the Ti states are located slightly above the Fermi level, whereas the Mn states cross it with spin-up component at the left interface and with down component at the right one. Besides, the states of neighboring oxygen are also cross the Fermi-level.

The performed structural reconstruction within the heterostructure leads to the electronic rearrangement as was discussed in the previous section. The arising electrostatic field leads to the shift of Ti states in the conduction band and oxygen states in the valence band higher in the energy scale as indicated in Figure 5(b). At the same time the density of states at the Fermi level did not change significantly neither left nor right interfaces. Overall, the distribution of density of states for two interfaces appear mirror symmetrical, but the change in the states position with respect to the ideal case is more obvious for left interface, where polarization vector and

magnetic moment are oppositely directed.

As soon as the polarization magnitude increases (Figure 5(c)), the distribution of the states changes dramatically. The most pronounced change is associated with Mn states. In plots for both interfaces the density of Mn states denoted by black curves increases significantly near the Fermi level. Moreover, minor spin components of Mn (spin-down for the left interface and spin-up for the right one) move down in the energy scale towards the Fermi-level. Major spin components at the Fermi-level increases the DOS, what indicates the increase of conductivity. The resulted magnitude there is approximately same for both interfaces. In addition to Mn, Ti states states in the conduction band move towards the Fermi-level so that the increased polarization or more ferroelectric layers might result in conducting Ti electrons.

The last considered case of oppositely directed polarization corresponds to the DOS presented in Figure 5(d). The distribution of Mn states is similar to the previous case with the DOS at the Fermi-level having slightly smaller magnitude. Oppositely, the distribution of Ti states changes in such a way that the magnitude of DOS decreases.

Overall, each case exhibits only one spin component on each interface at the Fermi-level, however, the change of the polarization direction does not switch that spin to the opposite orientation as was proposed in Ref. [4]. Indeed, the change of magnetic moments when the polarization changes is listed in the Table 2, but total magnetic moment change is inconsequential. Same is true for induced magnetization of Ti ions.

Table 2. Distribution of magnetic moments in $(LMO)_{4.5}/(BTO)_{3.5}$ heterostructure. Magnetic moments in μ_B are presented for all Mn and interfacial Ti ions, so that m1 and m4 correspond to interfacial moments, whereas m2 and m3 correspond to inner Mn ions. The signs of moments are given with respect to the z-axis as denoted in Figure 1. Two values in the cell means that the moments for two ions within the atomic layer are not identical.

LMO/BTO supercell	ion	m1	m2	m3	m4
polarization	Mn	$-3.941/-4.381$	4.035	-3.847	4.077/4.087
increased	Ti	$-0.024/-0.019$	–	–	0.018
polarization	Mn	$-4.386/-3.948$	3.866/3.846	$-3.844/-3.865$	3.946/4.384
opposite	Ti	$-0.016/-0.026$	–	–	0.026/0.017

4. Conclusion

In the paper structural, electronic and magnetic properties of two similar $LaMnO_3/BaTiO_3$ and $LaMnO_3/PbTiO_3$ ferroelectric/antiferromagnetic heterostructures were calculated by means of spin-polarized DFT calculations.

Similar features for both heterointerfaces were revealed associated with ferroelectric impact onto the electronic and magnetic states of LMO via electrostatic field. The last occurs during the structural relaxation and results in the build-up potential and electronic reconstruction. That was analysed and confirmed by plotting the distribution of potential as well as electron localization function. Moreover, the electronic reconstruction in the heterostructures caused the system to transit into a conducting state what was approved by density of states calculations. As for the magnetic properties it was revealed that the antiferromagnetic ordering within the LMO slab is preserved during the optimization. At the same time, Ti ions receive magnetic moments with same direction as neighboring interfacial Mn ions. The highest magnitude was found to be $0.925\,\mu_B$ for Ti and $4.099\,\mu_B$ for Mn, which are higher than in bulk (0 and $3.832\,\mu_B$,

respectively).

Lastly, the effect of polarization onto the electronic and magnetic properties was investigated. It was confirmed that increased polarization may increase the conductivity related mainly to the interfacial Mn states. It was also shown that polarization changes the magnitude of magnetic moments for both Ti and Mn ions, which might be used for spintronic purposes.

Acknowledgments

The research was supported by the government assignment for the FRC Kazan Scientific Center of RAS. Computational resources were provided by the Laboratory of Computer Design of New Materials and Machine Learning of Kazan Federal University.

References

1. Fredrickson K.D., Demkov A.A. *Phys. Rev. B* **91**, 115126 (2015)
2. Niranjan M.K., Wang Y., Jaswal S.S., Tsymbal E.Y. *Phys. Rev. Lett.* **103**, 016804 (2009)
3. Liu X., Tsymbal E.Y., Rabe K.M. *Phys. Rev. B* **97**, 094107 (2018)
4. Weng Y., Niu W., Huang X., An M., Dong Sh. *Phys. Rev. B* **103**, 214101 (2021)
5. Cao C., Chen S., Deng J., Li G., Zhang Q., Gu L., Ying T.P., Guo E.J., Guo J.G., Chen X. *Chinese Physics Letters* **39**, 047301 (2022)
6. Kabanov V.V., Piyanzina I.I., Lysogorskiy Yu.V., Tayurskii D.A., Mamin R.F. *Mater. Res. Express* **7**, 055020 (2020)
7. Niranjan M.K., Burton J.D., Velev J.P., Jaswal S.S., Tsymbal E.Y. *Appl. Phys. Lett.* **95**, 052501 (2009)
8. Duan C.G., Jaswal S.S., Tsymbal E.Y.*Appl. Phys. Lett.* **97**, 047201 (2006)
9. Niranjan M.K., Velev J.P., Duan C.G., Jaswal S.S., Tsymbal E.Y. *Phys. Rev. B* **78**, 104405 (2008)
10. Demkov A.A., Niu Q., Li Z., Shi J., Wang E. *Phys. Rev. B* **80**, 140415 (2009)
11. Baloni M., Sharma R.Ch., Singh H., Khan B., Singh M.K., Sati P.Ch., Thakur V.N., Kotnala R.K., Kumar A. *J. Alloys Compd.* **946**, 169333 (2023)
12. Ciucivara A., Sahu B., Kleinman L. *Phys. Rev. B* **77**, 092407 (2008)
13. Nguyen T.T., Yamauchi K., Oguchi T., Hoang N. N. *J. Electron. Mater.* **46**, 3808–3814 (2017)
14. Burton J.D., Tsymbal E.Y. *Phys. Rev. B* **80**, 174406 (2009)
15. Kresse G., Furthmüller J. *Comput. Mater. Sci.* **6**, 15–50 (1996)
16. Perdew J.P., Burke K., Ernzerhof M. *Phys. Rev. Lett.* **77**, 3865–3868 (1996)
17. Kohn W., Sham L.J. *Phys. Rev.* **140**, A1133–A1138 (1965)
18. Blöchl P.E. *Phys. Rev. B* **50**, 17953–17979 (1994)

19. Kresse G., Furthmüller J. *Phys. Rev. B* **54**, 11169–11186 (1996)

20. MedeA version 3.7; MedeA is a registered trademark of Materials Design, Inc., San Diego, USA.

21. Monkhorst H.J., Pack J.D. *Phys. Rev. B* **13**, 5188–5192 (1976)

22. Blöchl P.E., Jepsen O., Andersen O.K. *Phys. Rev. B* **49**, 16223–16233 (1994)

23. Methfessel M., Paxton A.T. *Phys. Rev.B* **40**, 3616–3621 (1989)

24. Dudarev S.L., Botton G.A., Savrasov S.Y., Humphreys C.J., Sutton A.P. *Phys. Rev. B* **57**, 1505–1509 (1998)

25. Calderon C.E., Plata J.J., Toher C., Oses C., Levy O., Fornari M., Natan A., Mehl M.J., Hart G., Nardelli M.B., Curtarolo S. *Comput. Mater. Sci.* **108**, 233–238 (2015)

26. Wang L., Maxisch T., Ceder G. *Phys. Rev. B* **73**, 195107 (2006)

27. Piyanzina I.I., Kopp T., Lysogorskiy Yu.V., Tayurskii D.A., Eyert V. *J. Phys.: Condens. Matter* **29**, 095501 (2017)

28. Piyanzina I.I., Eyert V., Lysogorskiy Yu.V., Tayurskii D.A., Kopp T. *J. Phys.: Condens. Matter* **31**, 295601 (2019)

29. Piyanzina I.I., Mamin R.F. *J. Supercond. Nov. Magn.* **35**, 2225–2229 (2022)

30. Kabanov V.V., Piyanzina I.I., Tayurskii D.A., Mamin R.F. *Phys. Rev. B* **98**, 094522 (2018)

31. Piyanzina I.I., Mamin R.F. *J. Mater. Sci.* **57**, 21620–21629 (2022)